Energy Conversion and Management 105 (2015) 167–177

Contents lists available at ScienceDirect

Energy Conversion and Management

journal homepage: www.elsevier.com/locate/enconman

An investigation of volute cross-sectional shape on turbocharger turbine under pulsating conditions in internal combustion engine

Mingyang Yang [a], Ricardo Martinez-Botas [b,*], Srithar Rajoo [c], Takao Yokoyama [d], Seiichi Ibaraki [d]

[a] School of Mechanical Engineering, Shanghai Jiao Tong University, Shanghai 200240, China
[b] Department of Mechanical Engineering, Imperial College London, SW72AZ London, UK
[c] UTM Centre for Low Carbon Transport in Cooperation with Imperial College London, Universiti Teknologi Malaysia, 81310 Johor, Malaysia
[d] Nagasaki Research and Development Center, Mitsubishi Heavy Industries, Ltd., Nagasaki 851-0392, Japan

ARTICLE INFO

Article history:
Received 12 September 2014
Accepted 13 June 2015
Available online 6 August 2015

Keywords:
Internal combustion engine
Turbocharging
Radial turbine
Volute

ABSTRACT

Engine downsizing is a proven method for CO_2 reduction in Internal Combustion Engine (ICE). A turbocharger, which reclaims the energy from the exhaust gas to boost the intake air, can effectively improve the power density of the engine thus is one of the key enablers to achieve the engine downsizing. Acknowledging its importance, many research efforts have gone into improving a turbocharger performance, which includes turbine volute. The cross-section design of a turbine volute in a turbocharger is usually a compromise between the engine level packaging and desired performance. Thus, it is beneficial to evaluate the effects of cross-sectional shape on a turbine performance. This paper presents experimental and computational investigation of the influence of volute cross-sectional shape on the performance of a radial turbocharger turbine under pulsating conditions. The cross-sectional shape of the baseline volute (denoted as *Volute B*) was optimized (*Volute A*) while the annulus distribution of area-to-radius ratio (A/R) for the two volute configurations are kept the same. Experimental results show that the turbine with the optimized *volute A* has better cycle averaged efficiency under pulsating flow conditions, for different loadings and frequencies. The advantage of performance is influenced by the operational conditions. After the experiment, a validated unsteady computational fluid dynamics (CFD) modeling was employed to investigate the mechanism by which performance differs between the baseline volute and the optimized version. Computational results show a stronger flow distortion in spanwise direction at the rotor inlet with the baseline volute. Furthermore, compared with the optimized volute, the flow distortion is more sensitive to the pulsating flow conditions in the baseline volute. This is due to the different secondary flow pattern in the cross-sections, hence demonstrating a direction for desired volute cross-sectional shape to be used in a turbocharger radial turbine for internal combustion engine.

1. Introduction

Increasing demands for vehicles with low CO_2 emission have forced the industry towards highly efficient engines. Engine downsizing is a proven method to improve the engine efficiency, which can effectively increases the power-to-weight ratio of vehicle propulsion, through reduction of either the cylinder volume or number, while still maintaining an equivalent power (with the original size engine). One of the key enablers for engine downsizing is turbocharging. Turbochargers are currently in their prime utilization period; where almost the whole transport industry is geared towards engine boosting and downsizing [1]. This directly pushes for increasing performance enhancement from conventional turbochargers and more often than not revisiting its design methodology. Turbine in a turbocharger is the important component which recovers energy from the exhaust gas of an engine. Hence there are many completed and on-going researches looking into turbocharger turbine performance improvement. It is well known that a turbine is subjected to pulsating flow, and how this feeds a steady-flow-design volute is a topic of interest for performance enhancement.

The primary function of a volute in radial/mixed flow turbine is to feed the rotor with uniform flow at the desired angle in order to optimize the performance. Design procedures of turbine volute based on steady conditions have been developed over few decades [2–10]. Most of the volute design efforts are on determining the optimal distribution of A/R in circumferential direction. The parameter A/R is the ratio of volute cross-sectional area and its

* Corresponding author.
E-mail address: r.botas@imperial.ac.uk (R. Martinez-Botas).

http://dx.doi.org/10.1016/j.enconman.2015.06.038
0196-8904/

Nomenclatures

A/R	ratio of volute cross section area and the radial of its center, mm
CFD	computational fluid dynamics
C_p	specific heat, J/(kg K)
MFP	mass flow rate parameter, kg/s · $\sqrt{K}$/Pa
P	pressure, Pa
PR	pressure ratio
RPM	rotations per minute
RANS	reynolds average Navies-Stocks equation
T	period of pulse, s
t	time, s

Greek letters

τ	torque, N m
r	ratio of specific heat
η	efficiency
ω	angular speed, rad/s
ρ	density, kg/m^3

Subscripts

0	start time of the pulse
i	inlet
e	exit
aver	average

centroid distance to rotational center. The distribution of A/R directly influences the flow angle distribution at the rotor inlet, thus has a significant impact on the turbine performance. On the same note, the volute cross-sectional shape is a key geometry which links the area and radius in the A/R. The usual industrial practice in deciding volute cross sectional shape is to find best compromise between the desired turbine performance and size/installation requirements. However, installation requirements take precedent in most cases, hence performance is sacrificed. Thus it would be beneficial for designers to know the exact influence of the volute cross-sectional shape on the turbine performance.

There are few documented investigations on the influence of volute cross-sectional shape on turbine performance or flow field. A direct comparison of volute flow information between a trapezoidal and approximately round shape was performed by Chen [5,8], via quasi-steady inverse method developed by Chapple et al. [3]. Chen [5,8] showed a clear difference in the angular momentum distribution around the circumference. However Chen [5,8] found little difference on the distribution of other flow parameters such as absolute flow angle and Mach number. Whitefield et al. [4,9,10] used the symmetrical trapezoidal shape in a series of volute investigations. Their results show the cir cumferential flow non-uniformity through calculation and experimental methods and it was attributed to disturbance at the volute tongue. They also indicated that the cross-sectional shape has its influence on the empirical coefficient of vortex (referring to '*m*' in the literature) in the volute, which then affects the flow distribution in circumferential direction. Suhrmann et al. [11] and Mishina et al. [12] designed and investigated a turbine volute with circular cross-sectional shape through 2-D model and detailed 3-D CFD method. Their results showed a non-uniform flow distribution in the radial and axial directions, which is closely related to the cross-sectional shape. Multiple investigations on the volute cross sectional shape have proven its considerable impact on radial turbine performance [13,14].

A turbocharger turbine is subjected to continuously pulsating exhaust flow from internal combustion engine. It has been shown that turbine behavior under the highly unsteady flow deviates from its equivalent steady performance [15–18]. There are limited documented investigations on the effects of volute cross-sectional shape on a turbine performance under pulsating flow conditions. One such research was by Hakeem et al. [19], where a volute with approximately trapezoidal cross-sectional shape was modified into an approximately elliptic shape. This was achieved by rounding the corners and consequently tested with a mixed-flow turbine rotor. Their experimental results showed a marginal improvement in the steady efficiency, but a significant improvement in the cycle averaged efficiency under pulsating flow conditions. The influence of volute cross-sectional shape on a mixed-flow turbine performance under pulsating flow conditions was demonstrated, but no further analysis was given.

The current paper aims to provide detailed analysis through experimental and CFD investigations into the influence of volute cross-sectional shape towards performance and flow characteristics of a turbocharger turbine under pulsating flow conditions. Detailed comparisons are conducted in order to quantify and demonstrate the mechanism by which the volute cross-sectional shape influences the flow characteristics and the turbine performance.

2. Experimental method

Experiments were carried out at the cold-flow turbocharger test-rig in Imperial College London – layout shown in Fig. 1. The turbine is driven by the compressed air which is heated up to 70 °C to avoid condensation after expansion. The pulsating air flow simulating engine exhaust flow is produced by a pulse generator, made of two chopper plates with specified cut-out shape. Turbine output power is absorbed by an in-house developed eddy current dynamometer [20] which enables wider performance map measurement, compared to conventional compressor loadings [15–17].

A turbocharger turbine with two versions of volute configurations (A and B – refer to Fig. 2), was tested under steady and pulsating flow conditions. The A/R circumferential distribution is same for both the volutes to maintain the similar swallowing capacity. The aspect ratio (b/h), which refers to the ratio of the width over the height of the cross-section, is used to describe the individual volute geometries, as shown in Fig. 2. For *volute A* the aspect ratio increases from 0.8 near the tongue (0°) to 2.6 at the end of volute passage (360°). Meanwhile the aspect ratio for *volute B* is 1.7 throughout the angular positions. The cross-sectional shape of the two volutes is shown in Fig. 2(a) and (b).

The volutes were fabricated by rapid prototyping in polycarbonate which can endure the pressure and temperature in testing. A Mitsubishi Heavy Industries (MHI) radial turbine rotor, as shown in Fig. 3(a), was used for the test of both the volute configurations. Geometries of the turbine rotor are shown in Table 1, and the test set up is shown in Fig. 3(b).

In steady flow testing, the turbine performance was evaluated at two speed lines as 30 and 40 kRPM. Mass flow rate is measured by the *McCrometer V-Cone* Flow meter (*dP* meter) with accuracy of ±0.5%. Flow pressure is measured with the scanivalve and temperature is measured by thermocouples. Output power is evaluated through load cell (torque) and speed. In pulsating flow testing,

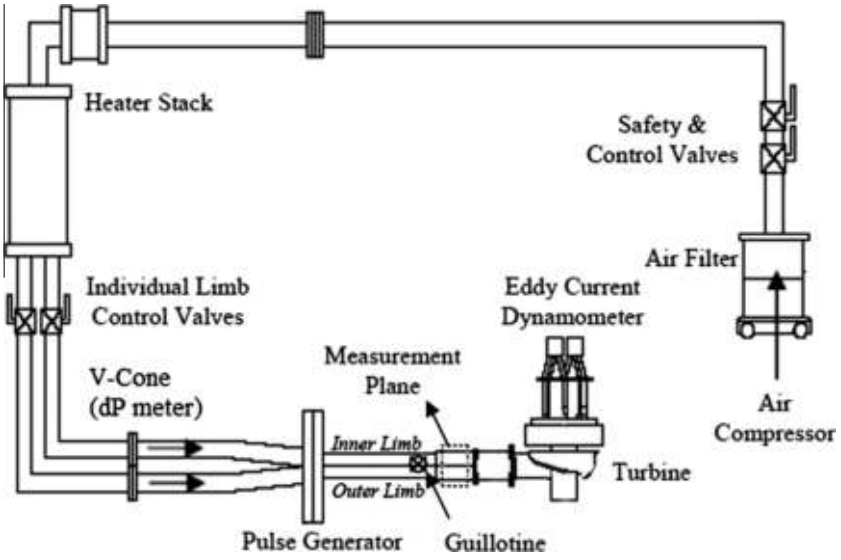

Fig. 1. Layout of the test-rig.

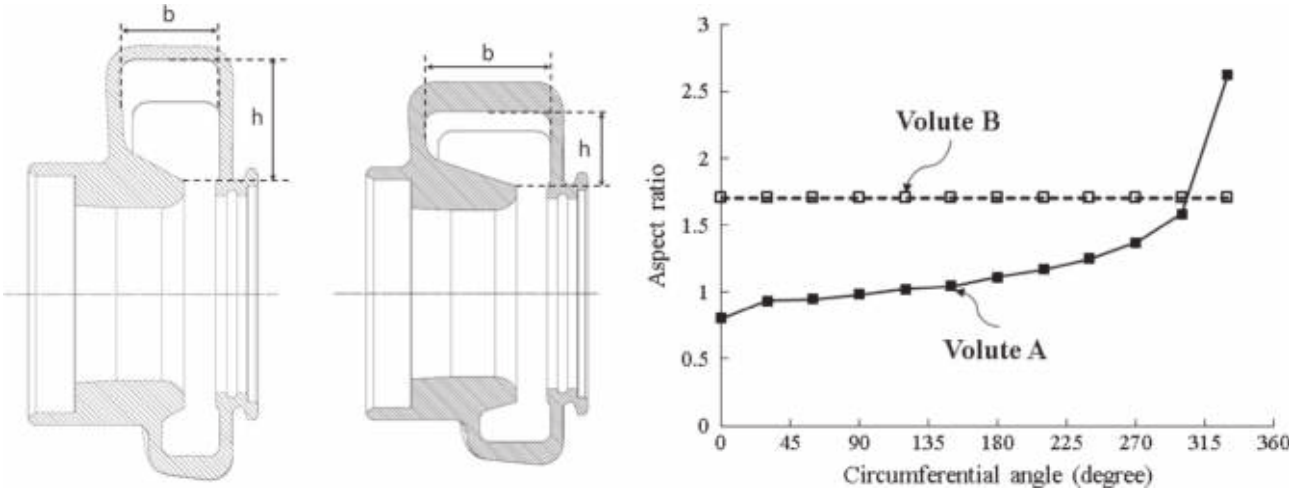

(a) *Volute A* (b) *Volute B* (c) Aspect ratio distribution of the two volutes

Fig. 2. Geometries of the two volutes.

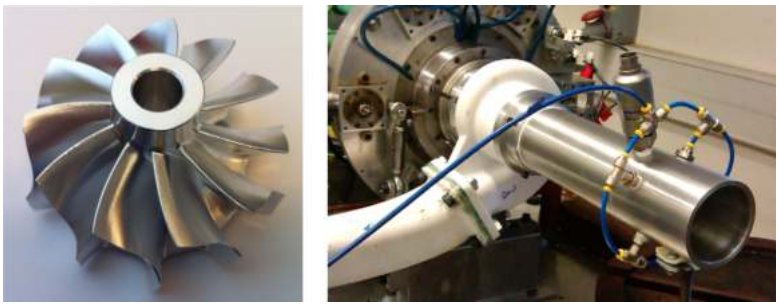

(a) MHI rotor (b) Test set up

Fig. 3. MHI turbine rotor and the test set up.

the turbine performance was evaluated at three different flow frequencies (20 Hz, 40 Hz and 60 Hz) and three different loads (low, middle and high loads) at the two speed lines. Instantaneous static pressure is measured at the measurement plane and turbine exit with *Schaevitz P704* pressure transducers. Meanwhile the instantaneous temperatures are evaluated with T-type thermocouples (mean) and the instantaneous pressure, via the isentropic relationship. Instantaneous torque is evaluated through rotor acceleration plus the average torque readings [20]. Instantaneous mass flow rate is measured by *Dantec 55P16 1-D* hotwire. The

Table 1
Main geometries of the MHI rotor.

Rotor geometries	
Inlet diameter of rotor	74.0 mm
Blade height of the rotor inlet	12.0 mm
Hub diameter at rotor exit	21.0 mm
Tip diameter at rotor exit	64.9 mm
Blade number	11

hotwire is calibrated with the *V-Cone* measurement in steady flow conditions covering the variation range of the temperature and mass flow rate under pulsating conditions.

3. CFD method

Computational Fluid Dynamic (CFD) method was employed to obtain flow field details of the volute configurations. In order to reduce the computational time and resources, a simplified unsteady CFD model was applied for both the two volute configurations. Only a single rotor passage was modeled to represent the whole turbine rotor in the method, as shown in Fig. 4(a). Meanwhile the inlet duct and the volutes were modeled upstream the rotor. Apart from the volute domain, meshes for the two configurations were kept the same to guarantee reliable comparisons. Moreover, topologies of the volute domains and the node number are also similar for the two configurations. Meshes of a volute are shown in Fig. 4(b). There are 1.6 million nodes in the whole turbine stage, consisted of 1.1 million nodes in the volute plus the inlet duct and 0.5 million in the rotor passage. Size of the first cell is set to be 5×10^{-2} mm which guarantees suitable y^+ for credible prediction. The mesh independence investigation was conducted on the rotor passage and the volute. The results show that the variation of the performance is limited in 0.2–0.3% as the mesh size is larger than 300 k and 700 k for the passage and the volute respectively. Therefore, the meshes applied for the investigation are considered to be independence from the prediction.

RANS equations were solved by the commercial CFD code. Spalart–Allmaras model was used to model the turbulence, which has been confirmed as a reliable model for the prediction of turbine performance [20]. Instantaneous total pressure and total temperature from experiments were imposed as the inlet boundary conditions. Meanwhile the averaged static pressure at turbine exit was imposed as outlet boundary condition. Adiabatic, non-slip wall condition was applied for the solid wall surfaces.

In order to capture the interaction between the volute and rotor, the interface between the passage and volute was treated with 'phase lagged' method. For a single passage, there are two periodic interfaces which connect the two passages at vicinity, as shown in subfigure (a). In the 'phase lagged' method, flow parameters on the downstream interface are determined with the results of previous pitch. Meanwhile for the upstream interface they are determined with the results of one full rotor rotation before. Therefore, the whole rotor can be modelled by a single passage via this method and unsteady phenomena can be simulated. Unsteady flow in the rotor can be predicted given that the flow in the rotor does not vary dramatically in a full rotation, which is a reasonable approximation for most of the pulsating conditions. More importantly, the calculation time reduces significantly by simplifying the whole rotor into a single passage.

Dual time steps method was applied for the unsteady calculation. There are 55 time steps in a full rotation (6.5° per step), which is coarse for studying flow details in the rotor, but adequate for flow in the volute, which is satisfactory to the current research. 40 inner iterations are conducted in each time step to guarantee a reasonable convergence. Well converged steady results were employed as the initial conditions of the unsteady calculation. The calculation is considered to be converged when the predicted pulse of flow parameters are well repeated for several pulse periods.

4. Results and analysis

4.1. Experimental test results

Swallowing capacity of the two volute configurations were measured under steady flow conditions at 30 kRPM and 40 kRPM. The pressure ratio and the mass flow rate parameter (MFP) are defined as Eqs. (1) and (2):

$$\mathrm{PR} = \frac{P_{t\_i}}{P_{s\_e}} \tag{1}$$

$$\mathrm{MFP} = \frac{m \cdot \sqrt{T_{t\_i}}}{P_{t\_i}} \tag{2}$$

Fig. 5(a) shows comparison of the two volute configurations at two rotational speeds. In order to fairly compare the two volute configurations, it is important to maintain the swallowing capacity, which was achieved through the same A/R distribution. As seen in

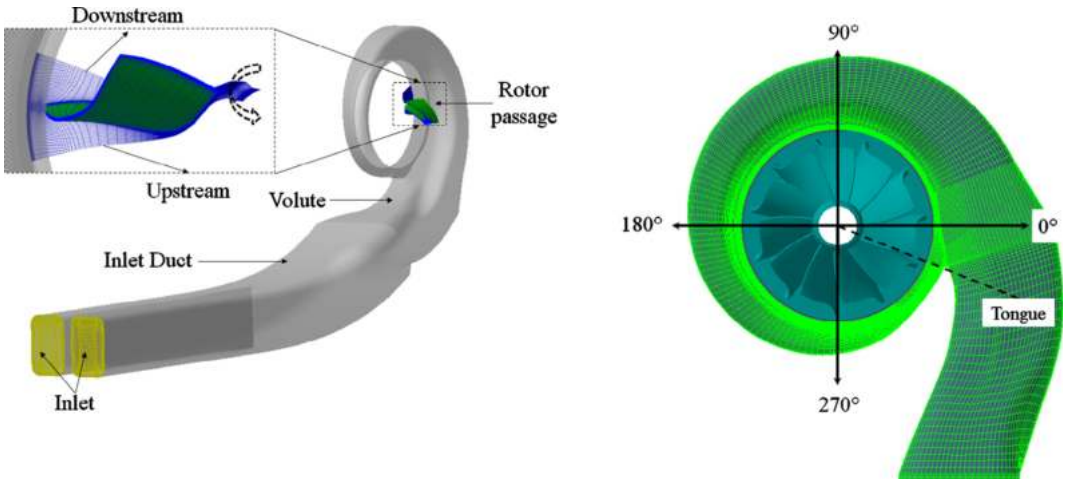

(a) Mesh of turbine for unsteady CFD (b) Mesh of volute

Fig. 4. Mesh of the turbine for CFD analysis.

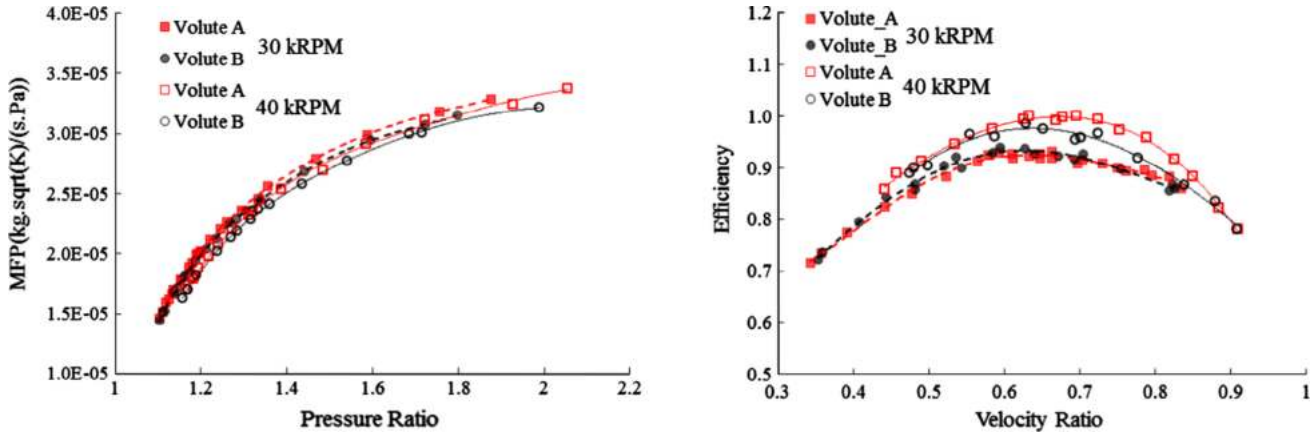

(a) Swallowing capacit y (b) Normalized efficiency

Fig. 5. Turbine performance comparison under steady conditions.

Fig. 5(a), mass flow rate parameter for both the volutes are not entirely on-top each other, but the difference is small (probably due to cross sectional shape). MFP for *volute B* drops slightly compared with *A*, by about 2% on average for both the speeds. Fig. 5(b) shows the turbine efficiency for *volute A* and B which is normalized with the peak efficiency of *volute A* at 40 kRPM. The efficiency and the velocity ratio are defined as Eqs. (3) and (4):

$$\mathrm{VR} = \frac{U}{\sqrt{C_P \cdot Tt_i \cdot \left(1 - \mathrm{PR}^{\frac{1-\gamma}{\gamma}}\right)}} \tag{3}$$

$$\eta = \frac{\tau \cdot \omega}{m \cdot C_p \cdot Tt_i \left(1 - \mathrm{PR}^{\frac{1-\gamma}{\gamma}}\right)} \tag{4}$$

The efficiency is similar for both the volutes at 30 kRPM, while at 40 kRPM volute A is marginally more efficient, especially at low load conditions. It is inferred that the swallowing capacity of the turbine is not sensitive to volute cross-sectional shape. However, the cross sectional shape the influence on the efficiency under steady conditions is enhanced as the turbine speed increases.

After the steady flow evaluation, turbine performance was then measured under pulsating conditions. There is a time lag between the turbine input isentropic power and the actual output power, due to the energy propagation time through the turbine. Thus the instant efficiency heavily relies on phase shifting between the input and output power, thus the debatable characteristic length. Therefore, cycle average parameters over a pulse period are used for the performance analysis. The definition of cycle average efficiency is given in Eq. (5).

$$\eta_{ave} = \frac{\int_0^T (\tau \cdot \omega) dt}{\int_0^T \left(m \cdot C_p \cdot T_0 \cdot \left(1 - \mathrm{PR}^{\frac{1-\gamma}{\gamma}}\right)\right) dt} \tag{5}$$

Cycle averaged pressure ratio is defined to evaluate the mean turbine loading under pulsating flow conditions, as given in Eq. (6).

$$\mathrm{PR}_{ave} = \frac{\int_0^T P_{in} dt}{\int_0^T P_{out} dt} \tag{6}$$

Meanwhile cycle averaged mass flow rate parameter is defined to compare the turbine swallowing capacity under pulsating flow conditions, as given in Eq. (7).

$$\mathrm{MFP}_{ave} = \frac{\int_0^T MFP \cdot dt}{T} \tag{7}$$

Three turbine loads, referring as low, middle and high load, and pulse frequencies (20 Hz, 40 Hz, and 60 Hz) have been investigated in the testing. Fig. 6 compares the turbine cycle averaged performance at the different loads and pulse frequencies, given for 30 and 40 kRPM. The peak cycle averaged efficiency for both the volutes is achieved at middle load condition, which is similar to the steady performance. However, the efficiency of *volute A* is superior to *volute B* at most of the test pulsating conditions. *Volute A* is about 1.8 efficiency points higher on average and at maximum 4 points, operating at 60 Hz, low load condition and 30 kRPM. It is worth noticing that the steady efficiency at this speed is very similar for the two volutes, as shown in Fig. 5(b). This suggests *volute B* experience higher flow losses when operated under pulsating flow. Although the efficiency notably differs between the two volutes, the cycle averaged MFP versus the pressure ratio is close to each other at the two speeds, hence indicating the similar swallowing capacity. Moreover, the averaged swallowing capacity under pulsating conditions overlaps well on the steady curve at the two speeds, as shown in Fig. 6(b). Similar as steady conditions, the volute cross-sectional shape has larger impact on the efficiency than on the swallowing capacity under pulsating flow. Volute A demonstrates a better performance over Volute B at most of the pulsating operating conditions.

The hysteresis loop in the plot of MFP versus pressure ratio under pulsating flow is a classic turbocharger turbine phenomenon. The shape and the encapsulated area of the loop are the direct indications of wave dynamic and filling/emptying effect in a turbine. Fig. 7 compares the hysteresis loops for the two volutes at middle load and different pulse frequencies. The influence of the frequency on the loop shape, thus the turbine unsteady behavior is clearly demonstrated. Loop shape for both the volutes varies with frequencies, obviously due to different behavior of wave propagation/reflection. However, evolution of the loops with frequency in terms of shapes and the encapsulated area is very similar for both the volutes.

Fig. 8 further compares the hysteresis loops at the same frequency (60 Hz) but with different loads. In general the loops for both the volutes remain similar in shape but expand notably outwards and shift along the steady curves to the higher pressure ratio as the load increases. This clearly demonstrates the increasing mass imbalance in the turbine as load increases. However, the shape of the loops together with the variation trend is quite similar between the two volutes at different loads.

The overall comparison of the hysteresis loops for both the volutes at different conditions shows that wave action and mass

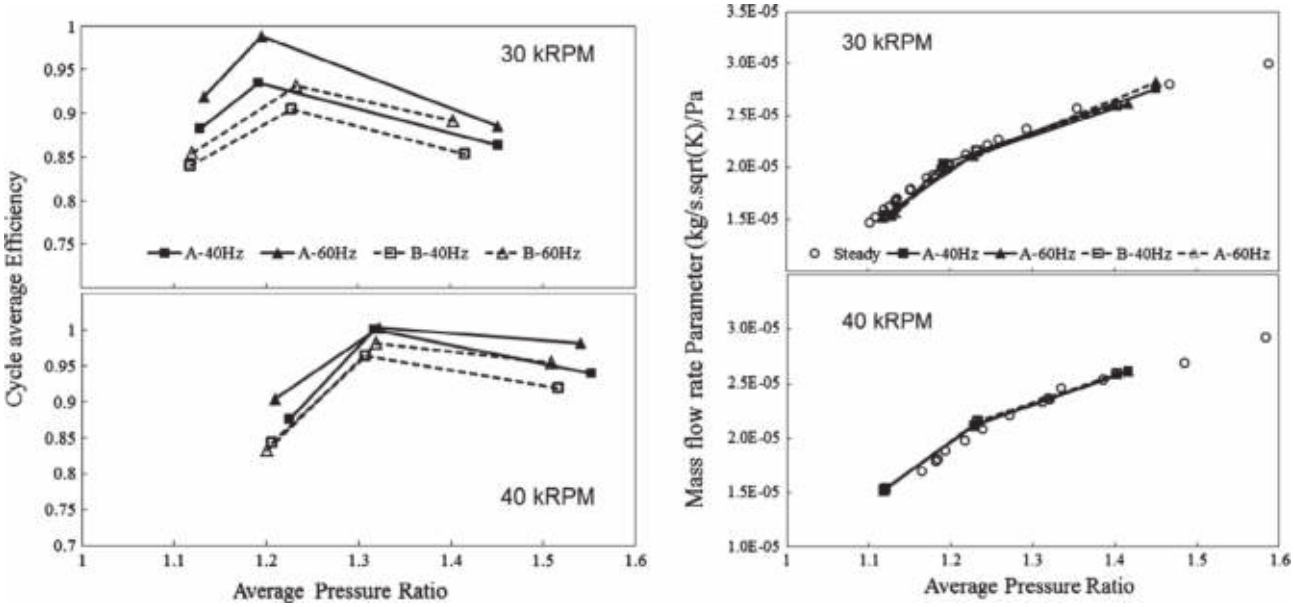

(a) Cycle averaged efficiency (b) Cycle averaged swallowing capacity

Fig. 6. Cycle averaged performance comparison at 30 and 40 kRPM for two volutes.

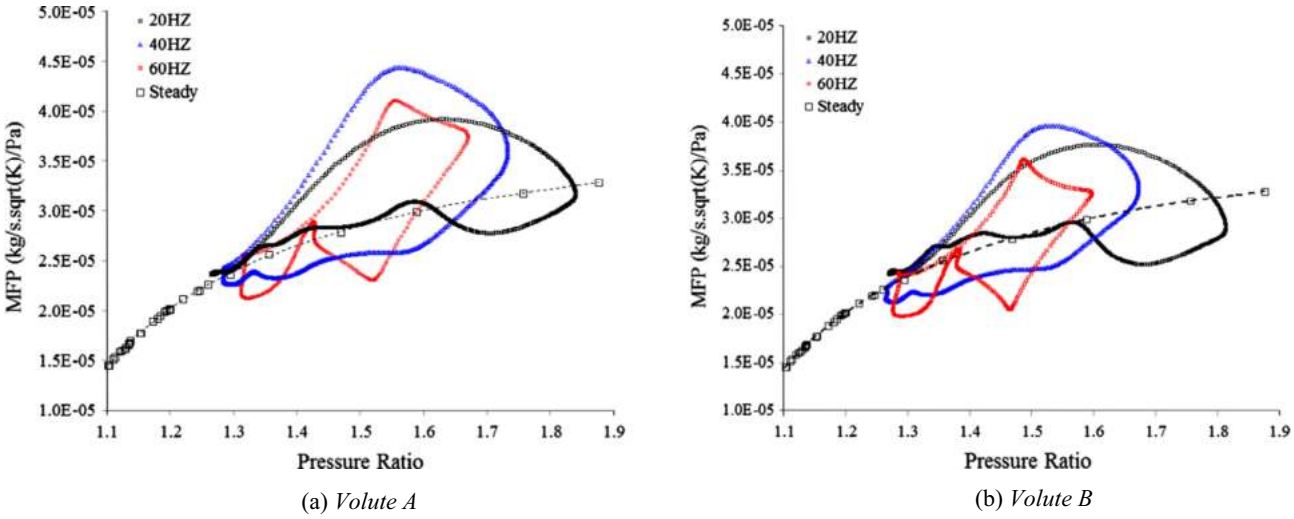

(a) *Volute A* (b) *Volute B*

Fig. 7. Hysteresis loops of the two volutes at different pulse flow frequencies and middle load.

imbalance are mainly influenced by the pulse frequency and the turbine load respectively. The volute cross-sectional shape has insignificant influence on the 'unsteadiness' in the turbine, which is in accordance with the cycle averaged swallowing capacity shown in Fig. 6(b). The length of the pulse propagation and the volume of the turbine system are considered to be two key factors of determining the corresponding wave dynamic and mass imbalance. But discrepancies of these two factors are almost negligible (0.1% for the volume for instance) for the two volute configurations. Therefore, the two volutes show similar swallowing capacity behavior under pulsating flow conditions although with different cross-sectional shapes. On the other hand, the advantage in the cycle averaged efficiency for *volute A* has been clearly shown. In order to allocate the reasons for the efficiency advantage of the volute, detailed flow field will be explored, as discussed in the following sections.

4.2. Flow field analysis

The unsteady CFD method was employed to investigate the details of flow field. The CFD model was validated with the experimental results for *volute A*. Fig. 9 compares the predicted and experimental results at 40 kRPM, 40 Hz and middle load condition. It can be noticed in Fig. 9(a) that CFD predicts a larger hysteresis loop, but the filling process is in good agreement with the test results. The discrepancy in the mass flow parameter during filling process is less than 1%. However, the discrepancy increases gradually as the emptying process begins. CFD under-estimates the mass flow rate in the emptying process in the turbine. As mentioned previously, the outlet boundary condition in simulation is the time averaged static pressure measured downstream the turbine rotor. This simplification naturally results in discrepancies between the simulation and experiments. Furthermore, another simplification

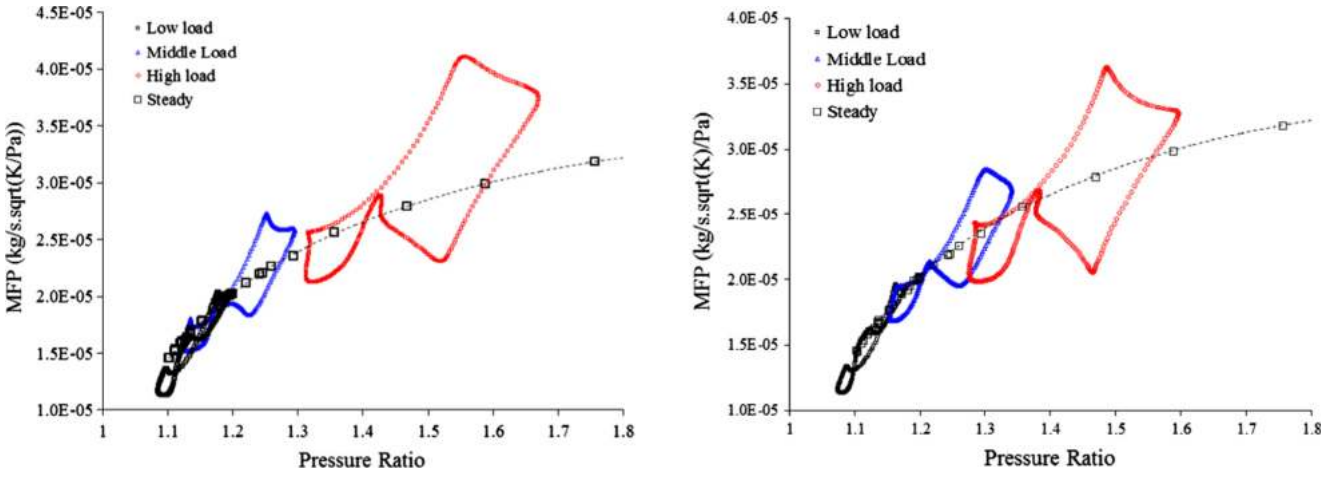

(a) *Volute A* (b) *Volute B*

Fig. 8. Hysteresis loops of the two volutes at different loads and 60 Hz.

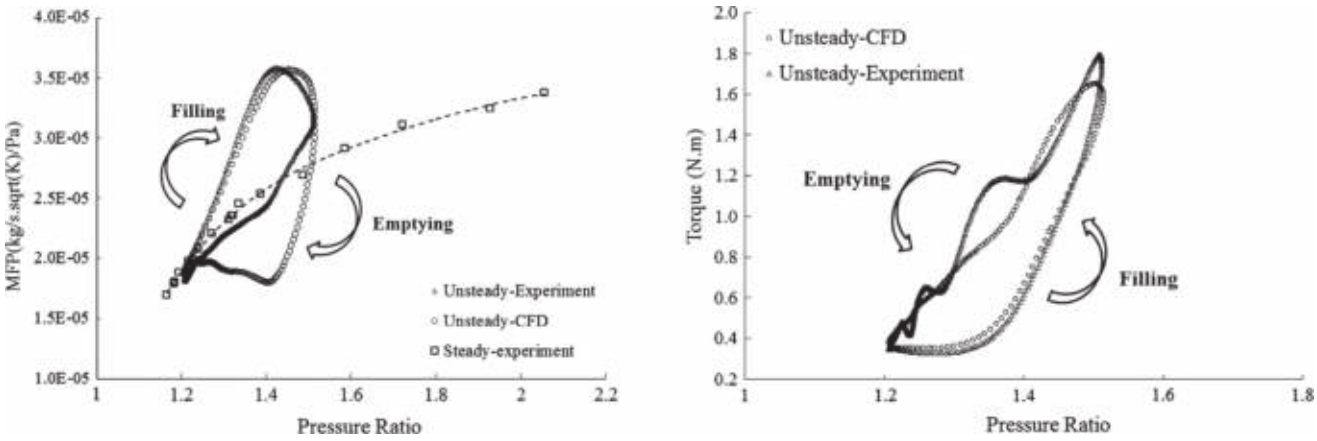

(a) Hysteresis loop of the swallowing capacity (b) Torque versus pressure ratio

Fig. 9. Validation of the unsteady CFD results at 40 Hz middle load condition for *volute A* (40 kRPM).

in the CFD method which treats the rotor as a quasi-steady component, is also considered to contribute to the discrepancies.

Fig. 9(b) shows the predicted torque compared with the measured value. The loop circles in an opposite direction to the swallowing capacity, resulting from the phase lag between the input power (relate to pressure ratio) and the output power (relates to torque). Similarly, the torque is well predicted in the filling process, but the discrepancy increases in emptying process – localized fluctuations observed in experiments are not predicted by CFD. The torque fluctuations in fact is produced by the speed variation under the pulsating flow condition. On the other hand, the speed in CFD is set to be constant during the pulse period, hence explaining the discrepancies seen in Fig. 9(b).

In conclusion, the simplified CFD method can reasonably predict the performance of turbine under pulsating flow conditions. The predicted flow field by the method is considered to be reliable for further discussion.

Table 2 compares the predicted cycle averaged performance for the two volutes under the same pulsating flow condition. The normalized cycle averaged efficiency of *volute A* is 2.3% higher than *voute B*, which is in good agreement with experiments shown in Fig. 6. In addition, the cycle averaged pressure ratio and mass flow rate are similar, which indicates similar swallowing capacity for the two volutes under pulsating flow conditions. Detailed efficiency (loss) break down in the turbine as well as flow field in the volute are analyzed in order identify reasons for the performance discrepancy between the volutes.

Table 2
Comparison of cycle averaged performance of the two volutes predicted by unsteady CFD.

	Volute A	*Volute B*
η_{ave} (–) (normalized)	1	0.977
PR_{ave} (–)	1.335	1.335
MFP_{ave} (kg/s sqrt(K)/Pa)	2.3×10^{-5}	2.39×10^{-5}

Reduction of the total pressure in a stator is a direct indicator of flow loss. Therefore, the difference of the total pressure at the volute exit will indicate difference in loss generation between the volutes. Fig. 10 shows the circumferential averaged total pressure at the exit of the two volutes, plotted against the pulse phase angle. The total pressure at the volute exit is seen to be lower than at the inlet during most of the pulse, indicating loss generated in the volute under pulsating flow conditions. Moreover, the magnitude of the total pressure is slightly lower for *volute B* compared to *volute A* near the peak. Therefore, higher loss is generated in *volute B* when approaching the peak of the pulse.

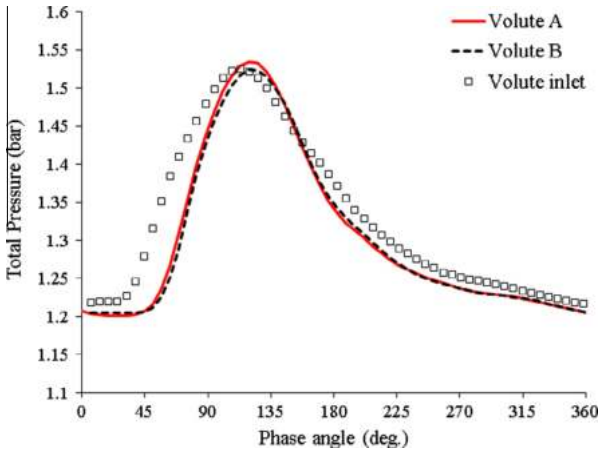

Fig. 10. Total pressure at the exit of the volutes.

Fig. 11 further compares the entropy distribution (referencing to ambient condition) in the cross-section at 0° and 180°, at the peak of pressure pulse. Most of the high entropy region is near the wall for both the volutes. Since *volute B* has smaller sectional area (and smaller radius of area centroid), the average velocity is higher compared to *volute A*, thus more flow loss is generated by friction. Moreover, the highest entropy is generated near the sharp corner at exit of both the volutes due to a step flow. However, the region with high entropy is much larger in *volute B* at 0° cross-section, indicating higher loss in the volute. Close scrutiny shows the recirculation region, indicated by the reversed velocity vector, is generated near the sharp corner in both the volutes, but the size and strength of the recirculation are much larger in *volute B*.

The distinction of the loss generation in the volutes can be related to the flow pattern in their cross-sections. Fig. 12 compares the secondary flow pattern in the cross-section at 0° location, at the peak inlet pressure condition. There are mainly two vortex structures (referring as *V*1 and *V*2) in the section for both the volutes, but the difference is evident. For *volute A*, the cores of the vortex are near the upper and lower wall of the section respectively, and they both stretch in radial direction. Meanwhile for *volute B*, the vortex *V*1 is aligned with the vertical wall and stretches in axial direction. Furthermore, the size of *V*1 is larger in *volute B*, thus the secondary flow is more profound in *volute B*. The interface between *V*1 and *V*2 can be clearly observed in *volute B*, as shown in Fig. 12. Interestingly, compared with Fig. 11(b), *V*1 and *V*2 separation is in accordance with the interface between the high entropy and low entropy region.

Comparison of the flow pattern near the volute exit in Fig. 11 shows that the flow distribution is quite different in the axial direction in two volutes. It is apparent that the discrepancy is caused by the different secondary flow pattern in the cross-sections. It is also expected that the rotor inlet flow condition will be different in spanwise direction, which will be discussed in detail.

Table 3 compares the breakdown of efficiency in the turbines. It can be seen that the difference of cycle averaged efficiency is mainly contributed by the rotor, while the volute only contributes to about 0.3%. Thus the performance difference between the two volute cross-sectional shape is not mainly caused by flow loss in the volute. Instead, the different rotor performance dominates the influence of cross-sectional shape under pulsating conditions. This phenomenon needs to be clearly understood via further investigations.

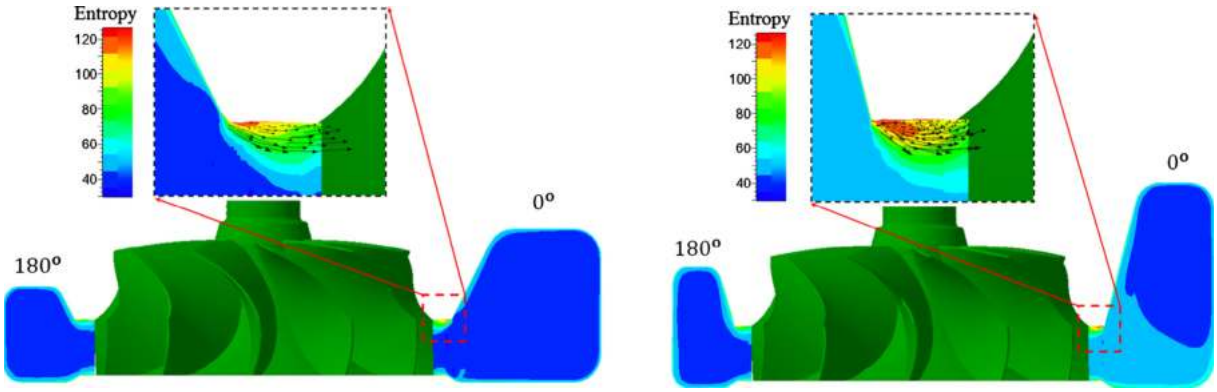

(a) *Volute A* (b) *Volute B*

Fig. 11. Entropy distribution in the volute sections.

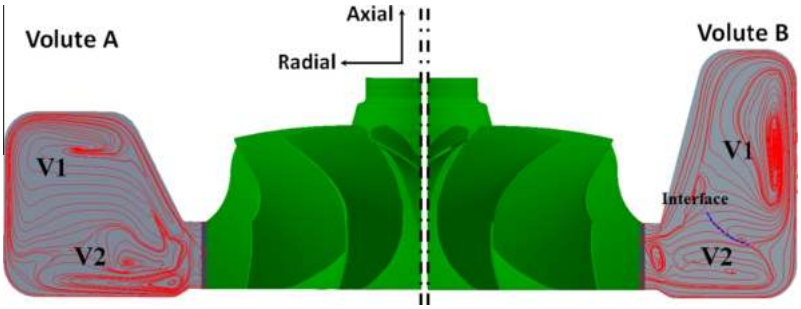

Fig. 12. Secondary flow of cross-section at 0°.

Table 3
Comparison of cycle averaged performance (normalized) of the two volutes.

	Volute A	*Volute B*	Discrepancy (%)
$\eta_{\text{ave-all}}$ (−)	0.907	0.886	2.1
$\Delta\eta_{\text{volute}}$ (−)	0.093	0.096	0.3
η_{rotor} (−)	1	0.982	1.8

Fig. 13 compares the absolute flow angle distribution in the circumferential direction at three axial locations and three instances in the pulse for the two volutes. These locations are near the hub (10% blade height), midspan and near the shroud of the rotor inlet (90% blade height). It can be seen that the flow is highly distorted in circumferential direction for both the volutes, which is apparently caused by the volute tongue. More importantly, the flow is obviously distorted from the hub to shroud, indicated by the

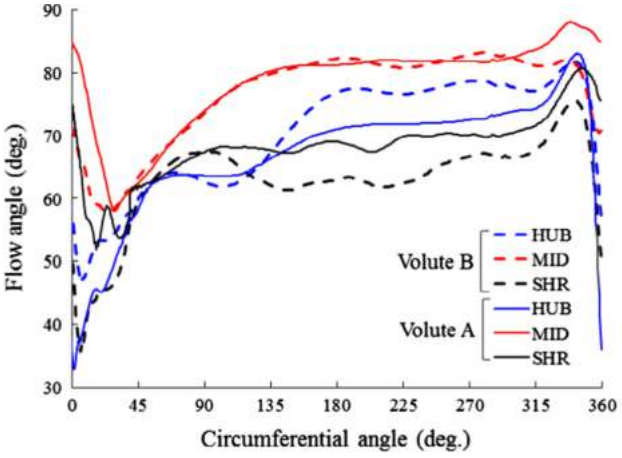

(a) Flow angle at A

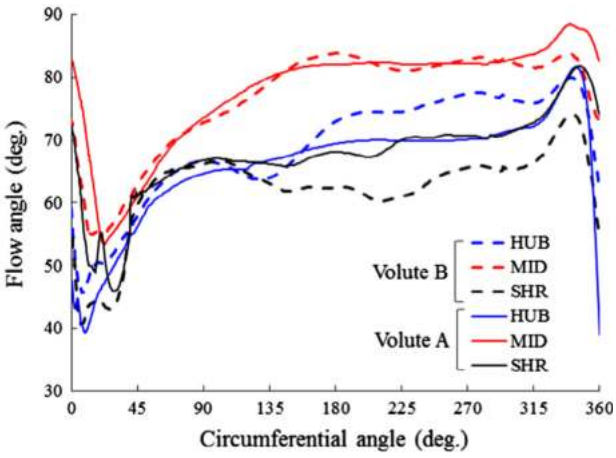

(b) Flow angle at B (peak)

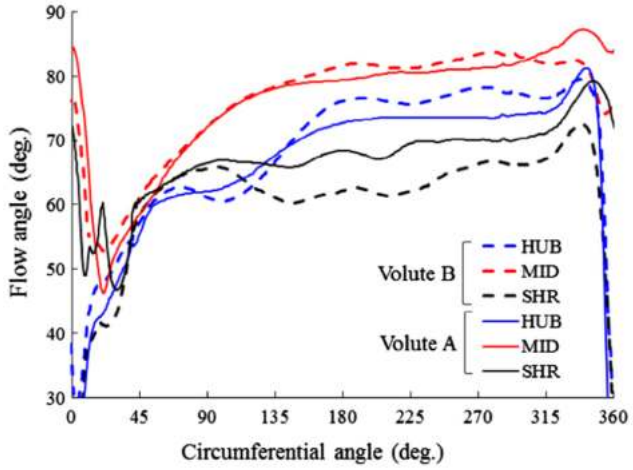

(c) Flow angle at C

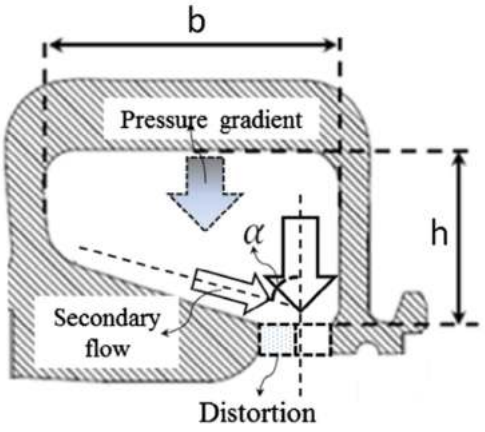

(d) Sketch of generation of distortion

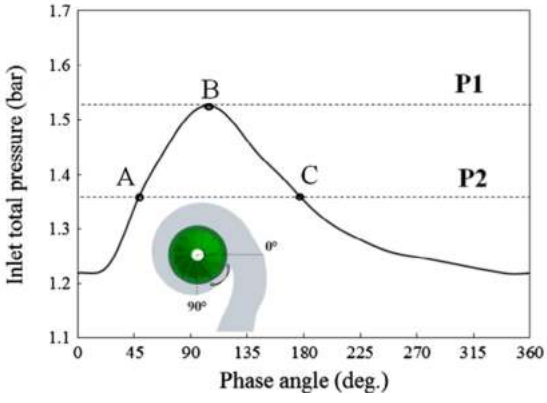

(e) 3 operational conditions for analysis

Fig. 13. Circumferential absolute flow angle distribution near the hub, midspan and shroud of the rotor inlet at the pulsating condition, 40 kRPM.

different flow angle distributions at the three blade heights. The flow angle variation is more profound from hub to shroud in *volute B*, showing more severe flow distortion. Similar flow phenomenon can be observed at other two locations as well.

There is usually an evident pressure gradient in radial direction in a volute cross section, which drives the flow to the volute exit. Considering the secondary flow pattern in a section, the flow migrates gradually inwards to the volute exit, as shown in Fig. 13(d). Since the exit of the volute is near the hub side, the rectangular shape of the cross-section forces the secondary flow near the lower wall to turn a certain angle (α) to align and combine with the main flow near the shroud side. This results in flow distortion at the vicinity of shroud, and this phenomenon has been clearly demonstrated by other researchers. Magnitude of the distortion is closely related with the turning angle α, which is determined by geometries of the cross sectional shape. For the volute with higher aspect ratio, the angle α is larger and thus produces more severe span-wise flow distortion. Furthermore, the flow angle distributions at three instances in the pulse are very similar, but the span-wise distortion is enhanced at the peak (subfigure (b)). Secondary flow in the volute cross section is amplified by the higher load thus resulting in more severe flow distortion.

Fig. 14 shows the circumferential flow angle distribution at the exit of the two volutes under steady and pulsating conditions. The distribution was taken at point A, as shown in Fig. 13, where the area averaged total pressure at inlet of the volute is the same as in the equivalent steady condition. This is to eliminate the influence of pulse propagation through the duct under pulsating flow condition for the steady/unsteady comparison. For both the *volutes A* and *B*, differences between the distributions at steady and unsteady conditions are small at shroud and middle span, but becomes significant at the hub. Moreover, most of the

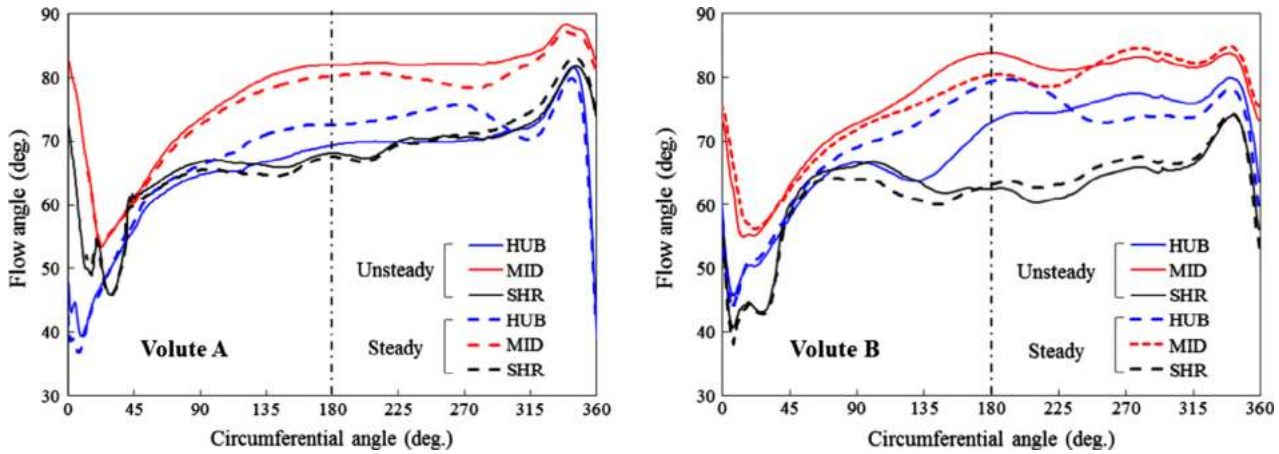

(a) *Volute A* (b) *Volute B*

Fig. 14. Circumferential absolute flow angle distribution near the hub, midspan and shroud of the rotor inlet at pulsating and the steady conditions, 40 kRPM.

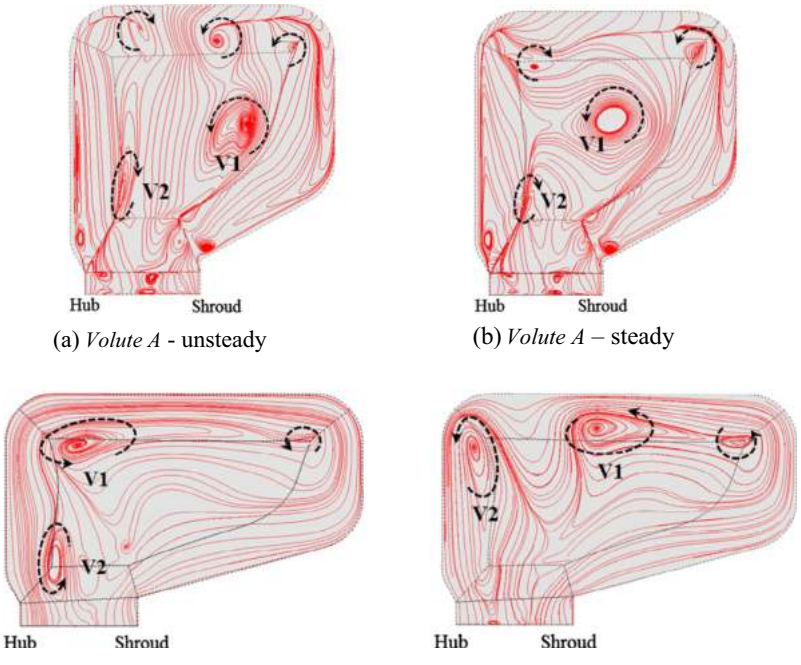

(a) *Volute A* - unsteady (b) *Volute A* – steady

(c) *Volute B* - unsteady (d) *Volute B* – steady

Fig. 15. Secondary flow in the cross sections of the two volutes at steady/unsteady conditions.

discrepancies exist in the range from 90° to about 315°. On the other hand, flow distortion in the circumferential direction (which is apparently caused by the volute tongue) is similar between the steady or unsteady conditions, given that the same pressure is imposed at the volute inlet.

Therefore, it can be concluded that the pulsating flow condition has evident impact on the span-wise distortion, but it has little influence on the circumferential distortion. The flow in the volute with a shape of higher aspect ratio (*volute B*) is more sensitive to the pulsating flow condition, especially near the hub region. This phenomenon is caused by the different secondary flow patterns in the cross-sectional shape. Fig. 15 compares the secondary flow structures under steady and pulsating flow conditions for both volutes at 180° (referring to Fig. 4). From Fig. 15 it can be seen that the flow pattern for *volute A* is relatively similar at steady and pulsating flow conditions. The topology and the relative locations of vortexes in the cross section are similar between the steady and pulsating flow conditions, including a main vortex in the middle of the section and several small corner vortexes. However, significant difference can be observed in *volute B* operating under pulsating flow condition. Although the topology of the vortexes is similar, the main vortex *V*1 migrates to the wall of hub side and pushes the counter-clockwise vortex *V*2 to migrate along the hub wall to the volute exit. Vortex *V*2 imposes a larger extra radial component on the main velocity vector, resulting in smaller flow angle near the hub at the volute exit, as shown in Fig. 14.

Comparisons in Fig. 15 show that the flow field in *volute A* updates faster when the inlet condition varies (pulsating flow), thus resulting in similar flow pattern as the corresponding steady condition. However, the flow pattern in *volute B* deviates from the corresponding steady condition when subjected to pulsating flow. An important observation is that the size of the vortexes in *volute B* is in general larger than in *volute A*. Therefore, the vortexes has larger 'inertia' in *volute B* and hence responses more slowly under pulsating flow, compared to the smaller vortexes in *volute A*. In conclusion, the distinct volute cross-sectional shape produces the difference of secondary flow pattern in the volute sections. This results in the different response time of the flow field under pulsating conditions, due to the inertia of the vortex, hence the different flow distributions along the spanwise at the inlet of the turbine rotor.

5. Conclusions

The volute of a turbocharger turbine is designed to feed the rotor with flow at a suitable direction and magnitude to obtain optimized performance. This paper presents the flow investigation in volute based on a nozzleless radial turbocharger turbine under pulsating flow conditions via experiments and numerical methods. The performance of baseline *volute B* and the cross-sectional-shape-optimized *volute A* are compared in the current investigation. Three conclusions are drawn as following:

(1) The cycle averaged efficiency is higher for the optimized volute (*volute A*) at most of the tested pulsating flow conditions. Specifically, the average efficiency improvement with *volute A* is about 1.8 points covering three frequencies (20 Hz, 40 Hz, 60 Hz) and three loads at 30 kRPM. However, the cycle averaged swallowing capacity is hardly influenced by the cross-sectional shape or operation conditions, which all falls near the steady-state curve. Furthermore, the wave dynamic, indicated by the shape of the loops, in the turbine is not sensitive to the volute cross-sectional shape. On the other hand, the mass imbalance in the turbine, indicated by the area covered by the loops under pulsating flow conditions, is noticeably influenced by the cross-sectional shape.

(2) Higher total pressure loss is generated in baseline *volute B* during a pulse cycle. This is caused by the sharper corner and flatter cross-sectional shape which enhance the development of secondary flow and hence higher loss generation. Deterioration of the turbine rotor performance is the major reason for the lower efficiency for *volute B*. It is caused by the more distorted flow distribution in spanwise direction at the volute exit.

(3) Flow field in the cross-sectional shape with the baseline volute (*volute B*) is more sensitive to the pulsating flow in terms of the distorted spanwise flow distortion referring to the corresponding steady condition. It results from the larger size of vortexes in the section which responses much slowly to the inlet pulsating conditions.

References

[1] Wei H, Zhu T, Shu G, Tan L, Wang Y. Gasoline engine exhaust gas recirculation – a review. Appl Energy 2012:534–44.

[2] Bhinder FS. Investigation of flow in the nozzleless spiral casing of a radial inward-flow gas turbine. In: Pro. Inst. Mech. Eng.; 1969.

[3] Chapple PM, Flynn PF, Mulloy JM. Aerodynamic design of fixed and varied geometry nozzleless turbine casings. J Eng Power 1980;102.

[4] Whitefild A, Mohd Noor AB. Design and performance of vaneless volutes for radial inflow turbines Part 1: non-dimensional conceptual design considerations. J Power Energy 1994;208.

[5] Chen H. Design methods of volute casings for turbocharger turbine applications. J Power Energy 1996;210.

[6] Abidat M, Hamidou MK, Hachemi M. Design and flow analysis of radial and mixed flow turbine volutes. In: European conference on computational fluid dynamics; 2006.

[7] Gu F, Engeda A, Benisek E. A comparative study of incompressible and compressible design approaches of radial inflow turbine volutes. Proc Inst Mech Eng 2001;215.

[8] Chen H. A discussion on volute design method for radial inflow turbines. ASME paper, GT2009-59110; 2009.

[9] MacGregor SA, Whitefild A, Mohd Noor AB. Design and performance of vaneless volutes for radial inflow turbines Part 3: experimental investigation of the internal flow structure. J Power Energy 1994;208.

[10] Whitefild A, MacGregor SA, Mohd Noor AB. Design and performance of vaneless volutes for radial inflow turbines Part 2: experimental investigation of the meanline performance – assessment of empirical design parameters. J Power Energy 1994;208.

[11] Suhrmann JF, Peitsch D, Gugau M., Heuer T. On the effect of volute tongue design on radial turbine performance. ASME paper, GT2012-69525; 2012.

[12] Mishina I, Gyobu I. Performance investigations of large capacity centrifugal compressor. ASME paper, 78-GT-3; 1978.

[13] Baloni BD, Channiwala SA, Mayavanshi VK. Pressure recovery and loss coefficient variations in the two different centrifugal blower volute designs. Appl Energy 2012;90:335–43.

[14] Ayder E, Van den Braembussche R, Brasz JJ. Experimetnal and theoretical analysis of the flow in a centrifugal compressor volute. ASME paper, 92-GT-30; 1992.

[15] Rajoo S, Martinez-Botas RF. Variable geometry mixed flow turbine for turbochargers: an experimental study. Int J Fluid Mach Syst 2008;1.

[16] Copeland CD, Newton P, Martinez-Botas RF. A comparison of timescales with a pulsed flow turbocharger turbine. In: 10th Int. Conf. on Turbocharging and Turbochargers, Instn. of Mech. Engrs, London; 2012.

[17] Chiong MS, Rajoo S, Romagnoli A, Costall AW, Martinez-Botas RF. Integration of meanline and one-dimensional methods for prediction of pulsating performance of a turbocharger turbine. Energy Conserv Manag 2014;81.

[18] Galindo J, Tiseira A, Fajardo P, García-Cuevas LM. Development and validation of a radial variable geometry turbine model for transient pulsating flow applications. Energy Conserv Manag 2014;85:190–203.

[19] Hakeem I, Su CC, Costall A, et al. Effect of volute geometry on the steady and unsteady performance of mixed-flow turbines. Proc IMechE Part A J Power Energy 2007;221.

[20] Szymko S, McGlashan NR, Martinez-Botas R, et al. The development of a dynamometer for torque measurement of automotive turbocharger turbines. J Automob Eng 2007;221.